Absolute charge-exchange cross sections for the interaction between slow Xe^{q+} $(15 \leqslant q \leqslant 43)$ projectiles and neutral He, Ar, and Xe

N. Selberg, C. Biedermann,* and H. Cederquist
Department of Atomic Physics, Stockholm University, Frescativägen 24, S-104 05 Stockholm, Sweden
(Received 25 September 1996; revised manuscript received 5 June 1997)

We report measurements of absolute cross sections for single- and multiple-electron capture in slow collisions ($v \sim 0.1-0.2$ a.u.). Partial cross sections for simultaneous r-electron removal from the target and p-electron retainment by the projectile $\sigma^r_{q,q-p}$ are presented for the systems Xe^{q+}-B, B=He, Ar, and Xe ($15 \leqslant q \leqslant 43$). The results are also described in terms of electron-retainment ($\sigma_{q,q-p}$), electron-removal (σ^r_q), and total-reaction (σ_q) cross sections. Further, we deduce experimental single-electron-capture cross sections $\sigma^1_{q-1,q-2}$ for $Xe^{(q-1)+}$-B collisions from measurements on the Xe^{q+}-B system. The data are compared with earlier and more recent scaling laws and the extended classical over-the-barrier model. [S1050-2947(97)08511-9]

PACS number(s): 34.70.+e, 34.50.Fa

I. INTRODUCTION

The first multiply charged ion-atom collision experiment in the low-energy regime was performed by Thomson by 1913 [1]. He investigated single- as well as multiple-electron capture phenomena at this very early date. During the following decades, however, little work was done in this area and it was then mostly concentrated on single-electron retainment. That is, only one electron is finally captured by the projectile, although one or several electrons might have been transferred initially. It was not until more than fifty years later that the true nature of such a simple process was understood [2–5]. For instance, the two coincidence measurements reported in [3] and [4] for

$$A^{q+} + B \rightarrow A^{(q-p)+} + B^{r+} + (r-p)e^- \qquad (1)$$

revealed that true single-electron capture $r=p=1$ is the largest contributor to the single-electron-retainment cross section $\sigma_{q,q-1}$. However, an important part of $\sigma_{q,q-1}$ was found to be due to transfer ionization processes in which $r \geqslant 2$ and $p=1$. Slightly earlier, Müller and co-workers [6,7] reported important work on scaling laws for the retainment cross section $\sigma_{q,q-p}$ for $p=1-4$.

When the projectile charge is high, a full quantum-mechanical treatment of the charge-transfer process may become prohibitively difficult due to the large number of reaction channels involved. Instead, results are often discussed in the framework of various classical or semiclassical models. In 1985, Bárány *et al.* [8] extended the classical over-the-barrier model, developed for one-electron systems by Ryufuku *et al.* [9], to include also multiple-electron capture. Shortly thereafter Niehaus [10] published a more detailed model built on the same basic ideas.

With the introduction of more advanced ion sources during the 1980s, more selective and sophisticated experiments became possible. Absolute-cross-section data for slow ion-atom collisions with very highly charged projectiles $q \geqslant 15$ are, however, still rarely reported in the literature. The published experimental results from the time around the middle of the past decade are from Iwai *et al.* (Kr^{q+}-He, $7 \leqslant q \leqslant 25$) [11], Tawara *et al.* (I^{q+}-He, $10 \leqslant q \leqslant 41$) [12], Mann ($Ar^{q+}$-He and H_2, $4 \leqslant q \leqslant 15$, and I^{q+}-He and H_2, $5 \leqslant q \leqslant 27$) [13], and Andersson *et al.* (Xe^{q+}-He, $11 \leqslant q \leqslant 31$) [14]. These articles, except [14], mainly focus on one-electron removal from a two-electron target. Recently, the activity in this field has increased and several papers have been published by different groups: Vancura *et al.* (Ar^{q+}-He, H_2, and Ar, $8 \leqslant q \leqslant 16$) [15,16], Ali *et al.* (Ar^{q+}-Ar, $5 \leqslant q \leqslant 17$) [17], and Nakamura *et al.* (I^{q+}-Ne, Ar, Kr, and Xe, $q=10$ and 15) [18]. The latter work focused on multiple-electron capture from various heavier targets.

The primary aim with the present series of measurements was to provide cross-section data on single- and multiple-charge-transfer processes for both He and heavier targets. We thus report close to 300 absolute cross sections $\sigma^r_{q,q-p}$ for collision processes according to Eq. (1) with projectiles A=Xe and targets B=He, Ar, and Xe. This large set of data has then been used as a basis for discussions of models and scaling laws for electron-transfer cross sections in the present and in a separate article by Selberg *et al.* [19]. The latter article [19] is mainly devoted to a detailed presentation of a different scaling law for the absolute cross sections for removal of *exactly* r electrons from the target. This scaling law is consistent with the recent scaling law for removing *at least* r electrons by Kimura *et al.* [20].

The main experimental installation for coincidence measurements of the collision products in Eq. (1) are described in Sec. II A, while the procedure to calibrate the effective target lengths (different for different gases) is described in Sec. II B. The outline of the data analysis is given in Sec. III. In Sec. IV we present the partial cross sections $\sigma^r_{q,q-p}$ in tables. For the discussion and comparisons with models and scaling laws the data are reduced to total-reaction cross sections $\sigma^{\rm tot}_q$, r-electron-removal cross sections σ^r_q, and p-electron-retainment cross sections $\sigma_{q,q-p}$. Various aspects of the experimental results will be compared with re-

*Present address: Max Planck Institute of Plasma Physics, Berlin Branch, Mohrenstraße 40/41, D-10117 Berlin, Germany.

cently developed [19] and earlier scaling laws [6,7] and with the extended classical over-the-barrier model [8].

II. EXPERIMENTAL TECHNIQUES

A. The main (coincidence) experiment

The ^{136}Xe projectiles were provided by the electron-beam ion source CRYSIS at the Manne Siegbahn Laboratory in Stockholm. The ion source was operated in the stretched pulse mode ($\sim$150-ms-long pulses) with a repetition rate of 0.5–20 Hz. An electron beam of 150 mA produced Xe^{q+} ions with charge states ranging between 15+ and 43+, which were extracted at energies of $3.8q$ keV. Each ion pulse contained $10^{-9}-10^{-10}$ C distributed over $\sim 5-10$ charge states. In short, after selecting the desired ion charge state with a bending magnet the beam was directed towards a gas cell containing the target gas He, Ar, or Xe. The charge states of projectiles leaving the cell were analyzed by a hemispherical electrostatic analyzer and the projectiles were then detected by a position sensitive detector. The gas cell had a physical length of 7 mm and the diameters of the entrance and exit apertures were 0.5 and 1 mm, respectively. The recoil ions created in the extraction region (2 mm wide in the direction of the beam) in the center of the gas cell were directed to a time-of-flight spectrometer by means of a positive pusher potential.

We have measured the detection efficiencies ϵ_r for 1+ and 2+ recoils created within the extraction region. Both $\epsilon_r(1+)$ and $\epsilon_r(2+)$ were found to be $(19\pm 3)\%$ for He and $(24\pm 3)\%$ for Ar and Xe. We thus assume that the efficiency is the same for all recoil charge states. The low detection efficiencies are caused by five grids that the recoil ions have to pass before they hit the detector. Each grid has a transmission of $\sim$82% and the detector efficiency, indicated by the measured efficiency, is $\sim$70%.

In order to eliminate disturbing electric fields along the beam the projectile path through the chamber had to be shielded. This decreased the effective pumping speed in the region in front of the gas cell and thus increased the effective target lengths (different for the three targets), which were determined experimentally as described in Sec. II B. In Fig. 1 we show an image of the registered projectile spectra along the axis of energy (charge-state) dispersion for Xe^{25+}-Xe together with the time-of-flight spectra coincident with projectiles retaining one $(q-1)$ and two $(q-2)$ electrons.

B. Calibration of effective target lengths

An additional experimental arrangement was used for calibration of the effective target lengths for He, Ar, and Xe. The reason for introducing a second setup was simply that it was mounted on the beam line when it was realized that the nominal target length (7 mm) could not be used in order to deduce the absolute-cross-section scales for the measurements already performed with the original (main) experimental installation. The effective target lengths (different for different gases) in the original experimental setup was thus deduced by first calibrating the effective target lengths for the second (''calibration'') setup by means of Ar^{14+}-He and Ar^{14+}-Ar cross sections from the literature. In the next step we used these effective target lengths to measure the absolute charge-exchange yields (single-electron retainment by the projectile) for Xe^{31+}-He and Xe^{31+}-Ar again with the calibration setup. The effective target lengths for Ar and He *in the main experiment* were then determined by relating the absolute charge-exchange yields for Xe^{31+}-He and Xe^{31+}-Ar to the same quantities already measured with the main setup. The calibration setup was equipped with a gas cell (10 mm geometrical length) without recoil-ion extraction devices. The outgoing projectile charge-state distributions were recorded by means of a 180° hemispherical analyzer and a position-sensitive detector [21,22].

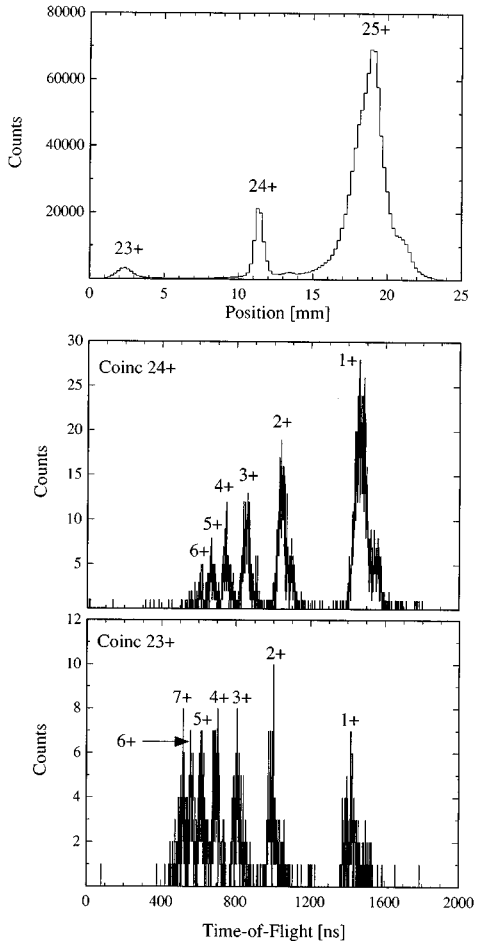

FIG. 1. Charge-state distribution of projectile ions in the main experiment as recorded on the position sensitive detector for Xe^{25+}-Xe collisions (top). To the right of the primary peak $(25+)$ there is a hump and to the left there is a tail. The treatment of these two features in the data analysis is discussed in the text. The time-of-flight spectra for recoil ions coincident with one- (Xe^{24+}) and two-electron retainment by the projectile (Xe^{23+}) are shown in the middle and the lower parts of the figure, respectively.

We measured the net one-electron-capture yields P_{q-1} in the calibration experiment for Ar^{14+}-He and Ar^{14+}-Ar collisions as functions of the pressures. When P_{q-1} is small, i.e., when $P_{q-1}\ll 1$, $P_{q-1}=\sigma_{q-1}\rho l$ is a fair approximation (ρ is the target density and l is the effective target length). The normalization to the absolute cross sections reported by Vancura *et al.* [15,16] yielded the effective target lengths for the calibration setup of 11.8 ± 0.5 mm and 10.8 ± 0.5 mm for He and Ar, respectively. The larger value for He is mainly due

to the fact that the gas flow from the cell is much higher for the lighter gas. The ratio between the flows of He (of mass m_{He}) and Ar (m_{Ar}) is $\sqrt{m_{\mathrm{Ar}}/m_{\mathrm{He}}}\approx 3.3$ with the same pressure in the cell for the two gases. Taking also the difference in pumping speeds (Balzers TPU 510) for He (570 l/s) and Ar (500 l/s) into account we note that the 0.8 mm extra target length (the geometrical length is 10 mm) for Ar ought to amount to 2.3 mm extra for the He target $[3.3\times 0.8\times(500/570)=2.3]$. The total effective target length $(10+2.3=12.3$ mm) expected from this reasoning is consistent with the measured value 11.8 ± 0.5 mm.

In the second step of the normalization procedure we measured the one-electron-retainment cross sections $\sigma_{q,q-1}$ for Xe^{31+}-He, Xe^{31+}-Ar, and Xe^{31+}-Xe on an absolute level (since the target lengths are now known) with the calibration setup. By relating these to the charge-exchange yields recorded at various pressures with the main experimental setup for Xe^{31+} projectiles we determined the effective target lengths in the main experiment to 18.6 ± 0.8 mm for He and 10.6 ± 0.5 mm for Ar. These values are considerably larger than the geometrical length of the gas cell in the main experiment (7 mm), which is due to the μ-metal shielding of the ion beam close to the gas cell causing serious reductions of the pumping speeds in this region. The shield used in the main experiment was different from the one used in the calibration setup. Again, the reason for the much longer He target becomes clear when considering the differences in gas flows from the cell and the pumping speeds of the turbopump. The 3.6 mm extra length for Ar indicates an extra length of 10.4 mm for He $[3.6\times 3.3\times(500/570)]$, where the factor 3.3 is due to the difference in flows for He and Ar at the same cell pressure. The result 17.4 mm $(7+10.4$ mm) is close to the experimental value 18.6 ± 0.8 mm. This large effective target length for He can be checked in a completely independent way since our present single-electron-capture cross section $(\sigma^1_{q,q-1})$ for Xe^{31+}-He (using the effective length 18.6 mm) is in agreement with the one reported by Andersson *et al.* [14], using the same cell without shield and consequently a shorter effective target length. Thus the present absolute effective target lengths in the main experiment are now firmly established for the He and Ar targets. For Xe this procedure could not be used and for simplicity we assumed that the effective length was equal to that of Ar.

III. DATA ANALYSIS

With the knowledge of the effective length (l) and density (ρ) of the gas target in the main experiment, it is possible to determine the absolute cross section for removal of r electrons from the target and retainment of p electrons to the projectile $\sigma^r_{q,q-p}$. This is done by comparing the number of events registered on the position sensitive detector in the peak corresponding to capture of p electrons to the projectile $N_{q,q-p}$ and the total number of registered events N_q. Multiplying this with the fraction of recoils with charge $r+$, $f^r_{q,q-p}$, in coincidence with projectiles of charge $(q-p)+$ we get

$$\sigma^r_{q,q-p}=\frac{N_{q,q-p}}{\Sigma_{t=0}N_{q,q-t}}\,\frac{f^r_{q,q-p}}{\rho l}=\frac{N^r_{q,q-p}}{\Sigma_{t=0}N_{q,q-t}}\,\frac{1}{\rho l}, \qquad (2)$$

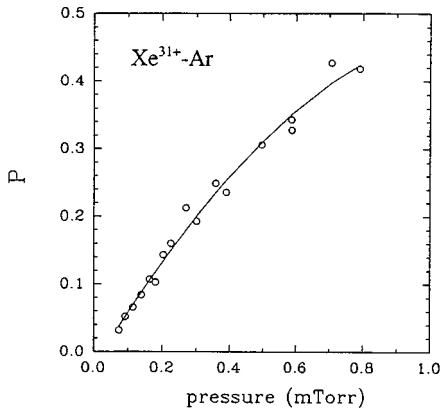

FIG. 2. Measured one-electron retainment yields P_{q-1} for Xe^{31+}-Ar collisions as a function of the target gas pressure in the calibration experiment.

where $\Sigma_{t=0}N_{q,q-t}=N_q$ is the total number of incoming ions. All these various peaks are well separated and ought to be fitted easily by Gaussian curves and hence the analysis ought to be trivial. However, as seen in Fig. 1, a tail is in between the primary peak and the $q-1$ peak and sometimes a side hump also appears close to the primary peak (in this case to the right). The inclusion or omission of these contributions in the primary peak intensity largely affects the result, sometimes by a factor of 2. We have, however, resolved this problem by using the information provided by double collisions (i.e., two consecutive collisions with different target atoms).

Absolute cross sections can also be determined directly from double-collision coincidences $(N^1_{q,q-2})$ using the formula

$$\sigma^1_{q-1,q-2}=\frac{N^1_{q,q-2}}{N^1_{q,q-1}}\,\frac{f^1_{q,q-1}}{\rho l}=\frac{N^1_{q,q-2}}{N_{q,q-1}}\,\frac{1}{\rho l}, \qquad (3)$$

where $N^1_{q,q-1}$ and $N^1_{q,q-2}$ are the measured numbers of singly charged recoil ions in coincidence with projectiles retaining one and two electrons, respectively. The total number of projecile ions retaining one electron $N_{q,q-1}$ is related to $N^1_{q,q-1}$ through $N^1_{q,q-1}=f^1_{q,q-1}N_{q,q-1}$, where $f^1_{q,q-1}$ is the fraction of singly charged ions in the recoil ion distribution for projectiles retaining one electron. The last form of Eq. (3) relies on the observation that $f^1_{q,q-1}\sim f^1_{q-1,q-2}$ (cf. Fig. 3) and resembles the last form of Eq. (2), which we used for extraction of cross sections $\sigma^1_{q,q-1}$ from single-collision events. This can be understood by observing that given that a $1+$ recoil ion is created in the extraction region, the other collision may be located anywhere in the target of thickness ρl. The method of extraction of cross sections $\sigma^1_{q-1,q-2}$ from double-collision events in the present setup is described in detail elsewhere [23].

From Fig. 1 it is clear that the $q-1$ and $q-2$ peaks are cleaner than the primary peak (q). Gating this spectrum with singly charged recoil ions reduces the weak tails and background around the two former peaks even further. We thus deduce single-electron-capture cross section for collisions $Xe^{(q-1)+}$-B with quantities measured for the system Xe^{q+}-B using Eq. (3).

TABLE I. Partial cross sections $\sigma^r_{q,q-p}$ for the processes $Xe^{q+}+He \rightarrow He^{(q-p)+}+He^{r+}+(r-p)e^-$ in units of 10^{-15} cm^2. In the cases where only single-electron-capture cross sections ($\sigma^1_{q,q-1}$) are given, the results are obtained by means of the double-collision method (cf. Sec. III B). The collision energy was $3.8q$ keV.

q	$\sigma^1_{q,q-1}$	$\sigma^2_{q,q-1}$	$\sigma^2_{q,q-2}$
30	11.1±1.4		
31	12.6±1.6	3.4±0.5	1.2±0.2
32	9.6±1.2	2.8±0.5	0.9±0.2
33	14.4±1.3	4.1±0.5	1.0±0.2
34	13.6±1.0		
35	13.5±1.3	3.7±0.4	1.0±0.1
36	13.6±1.5	3.2±0.4	1.4±0.2
37	14.2±2.0	3.2±0.5	1.4±0.3
38	11.8±1.4	5.9±0.9	1.6±0.3
39	17.6±3.1		
40	14.4±2.0	3.2±0.6	2.1±0.5
41	17.0±4.9		
42	16.4±3.4	4.6±1.4	2.2±0.8

In quite a few cases (when measurements were made for neighboring projectile charge states) it was possible to compare results from the double-collision method with those obtained directly using the single-collision data and formula (2). The agreement was excellent in most of the cases when the intensities due to the tail and the hump were omitted from the primary peak intensity in Eq. (2). This agreement also supports an assumption that was made implicitly here, namely, that the excitation produced in the first collision was relaxed before the second collision. This appears to be reasonable since typical lifetimes for the yrast states (which are the most long lived) lie in the subnanosecond regime, while a typical time between two collisions in the cell is of the order of 10 ns (considering the whole length of the cell). It cannot be completely ruled out that somewhat more long-lived metastable states with low excitation, which may be created in the relaxation cascades, could slightly influence the cross sections obtained with the double-collision method. Again, however, such effects cannot be very important since the double-collision results agree with those obtained using single collisions.

IV. RESULTS AND DISCUSSION

The partial cross sections $\sigma^r_{q,q-p}$ for reactions (1) are presented in Tables I, II, and III for the targets He, Ar, and Xe, respectively. The errors in the cross sections consist of the errors in the linear coefficients of the fits to the pressure dependences of the charge-exchange yields (cf. Fig. 3) and statistical errors in the determinations of the corresponding recoil-ion distributions. Additional absolute errors of ~10%, which are not included in Tables I–III, are due to the uncertainties in the absolute cross sections used for normalization (cf. Sec. II B).

The double-collision method has been used for the cases where only single-electron-capture cross sections are given. As can be seen in these tables, cross sections for removal of up to nine electrons from the target are reported as well as cross sections for retaining up to three electrons ($p=3$) on the projectile. For most of the collisions studied, however, we present data only for $p=1$ and $p=2$. The cases where we do have results for $p=3$ show that $\sigma_{q,q-1}$ and $\sigma_{q,q-2}$ are dominant in the total cross section. This is consistent with the results of Vancura *et al.* [16] and Raphaelian *et al.* [24], who have shown that $p=1$ and $p=2$ account for more than 95% of the total cross section.

A. Total-reaction cross sections, Q values, and capture states

Since the cross section for pure ionization of the target in the present velocity regime ($v \sim 0.2$ a.u.) is small [25], the total-reaction cross section should be very close to the total-electron-removal cross section. This means that it is possible to discuss the former cross sections in the framework of the extended classical over-the-barrier (ECB) model [8]. This model was developed in order to describe single- and multiple-electron removal in slow collisions between highly charged ions and neutral atoms. The active electrons experience a superposition of two Coulomb potentials originating from the projectile and target cores. As the projectile ion approaches the target the Coulomb barrier for the outermost target electron decreases. At a certain internuclear distance R_1 the first electron is assumed to be removed from the target to a quasicontinuum of states in the projectile. More electrons are succesively removed by the projectile if the internuclear distance continues to decrease. The critical distance where the top of the barrier becomes sufficiently low for removal of the rth electron is given by (in a.u.)

$$R_r = \frac{2\sqrt{r}\sqrt{q-r+1}+r}{I_r}, \tag{4}$$

where I_r is the ionization potential of the rth target electron. Using the absorbing sphere concept and assuming that no electrons are transferred back to the target, one arrives at a cross section for removal of the rth electron σ^r_q of

$$\sigma^r_q = \pi(R^2_r - R^2_{r+1}). \tag{5}$$

The total-electron-removal cross section is then the sum of all these, i.e.,

$$\sigma^{\mathrm{tot}}_q = \sum_r \sigma^r_q = \pi R^2_1. \tag{6}$$

This should be regarded as an upper limit of the cross section since the density of available capture states in the projectile is not invoked and further a 100% reaction probability is assumed for impact parameters smaller than R_1. In Ref. [19] we compared calculated [from Eqs. (4) and (6)] and measured total-reaction cross sections. The agreement was found to be well within ±20% in virtually all the 45 cases discussed in Ref. [19].

The total Q values for r-electron removal are given by the ECB model as

$$Q^{\mathrm{tot}}_r = \sum_r Q_r = \sum_r (E_r - I_r) = \sum_r \frac{q-(2r-1)}{R_r}, \tag{7}$$

TABLE II. Same as Table I, but with Ar as a target.

q	$\sigma^1_{q,q-1}$	$\sigma^2_{q,q-1}$	$\sigma^3_{q,q-1}$	$\sigma^4_{q,q-1}$	$\sigma^5_{q,q-1}$	$\sigma^6_{q,q-1}$
24	11.3±1.3					
25	10.9±0.9	5.3±0.5	3.5±0.4	1.2±0.1		
26	13.4±1.8	7.0±1.0	3.7±0.5	1.0±0.2		
27	13.7±1.6	6.6±0.9	4.1±0.4	1.1±0.2	0.4±0.09	
28	13.9±1.3	6.6±0.7	5.4±0.6	2.0±0.3	1.0±0.2	
29	5.9±0.4	3.3±0.3	2.3±0.2	0.8±0.1	0.5±0.06	0.3±0.05
30	15.2±1.4	6.1±0.7	3.7±0.5	1.7±0.3	1.0±0.2	
31	15.3±1.1	5.9±0.5	3.7±0.3	1.7±0.2	0.9±0.1	
32	12.3±1.9	4.5±0.8	2.5±0.4	1.3±0.2		
34	21.6±5.5					
35	18.9±2.1	5.7±1.0	4.8±0.8	1.3±0.4		
36	22.0±4.3					
37	18.6±2.3	5.4±0.9	3.1±0.6	1.2±0.2		
39	14.0±4.4					
40	16.7±2.6	5.4±1.2	1.6±0.5	0.7±0.3		
41	22.6±3.1	7.6±1.7	4.9±1.2	2.4±0.7	1.2±0.4	
42	24.0±4.5					
43	18.6±2.8	5.7±1.0	2.1±0.4	0.8±0.2		
q	$\sigma^2_{q,q-2}$	$\sigma^3_{q,q-2}$	$\sigma^4_{q,q-2}$	$\sigma^5_{q,q-2}$	$\sigma^6_{q,q-2}$	$\sigma^7_{q,q-2}$
25	0.4±0.07	0.8±0.1	1.0±0.1	1.0±0.12		
26	0.4±0.09	1.4±0.2	1.6±0.2			
27	0.2±0.06	0.6±0.1	0.8±0.2	1.4±0.2	1.2±0.2	0.7±0.1
28	0.9±0.2	1.2±0.2	1.1±0.2	1.4±0.2		
29	0.5±0.06	0.8±0.09	0.4±0.05			
30	1.6±0.3	1.9±0.3	1.8±0.3	1.9±0.3		
31	1.4±0.2	2.3±0.2	1.4±0.2	1.3±0.2		
32	1.6±0.3	2.3±0.4	1.1±0.2	1.2±0.2	1.0±0.2	
35	2.6±0.6	2.9±0.6	2.7±0.6	1.5±0.4		
37	2.3±0.5	2.2±0.4	1.6±0.4	1.2±0.3		
40	2.0±0.6	3.4±0.8	2.6±0.7			
41	1.8±0.6	6.0±1.4	2.8±0.8			
43	0.6±0.2	1.9±0.4	2.1±0.4			

where E_r is the total change in electronic binding energy on the projectile due to the transfer of the rth target electron. The Q_1 and $Q_2^{\rm tot}$ values have been measured directly by Cederquist *et al.* [22] for Xe^{q+}-He collisions in the charge-state regime $25 \leqslant q \leqslant 44$. According to the ideas of the ECB model, there should be a strong correlation between the Q_1 value and the total reaction cross section $\sigma_q^{\rm tot}$ through expressions (6) and (7). For the He target there should also be a similar relation between $Q_2 = Q_2^{\rm tot} - Q_1^{\rm tot}$ and σ_q^2, the absolute cross section for removing two electrons from the target. In Fig. 4 we plot the measured values of Q_1 and Q_2 from Ref. [22] as functions of $C_1 = (q-1)/\sqrt{^{ex}\sigma_q^{\rm tot}}$ and $C_2 = (q-3)/\sqrt{^{ex}\sigma_q^2}$, respectively, where the two latter quantities are obtained from the present absolute experimental cross sections. The line in the figure is a fit to the experimental points and its slope is $(2.1 \pm 0.2) \times 10^{-7}$ eV cm, which is close to the one expected from the model ($\sqrt{\pi} \times 10^{-7}$ eV cm).

In Ref. [22] we used the direct measurements of mean $Q_1^{\rm tot}$ values to deduce the principal quantum numbers populated in single-electron capture. The correlation between measured Q values and measured cross sections in Fig. 4 shows that it should be possible to deduce the capture n states directly from absolute-cross-section measurements (although with larger uncertainties than from measured Q values). In Fig. 5 we show the semiempirical effective quantum numbers n_1^* and n_2^* for all three targets deduced from cross sections results and the ECB model. The corresponding quantities deduced directly from the ECB model are shown as dashed lines in Fig. 5. The n_1^* values for He, obtained from the measured Q_1 values [22], are also shown in this figure and they are slightly lower than the n_1^* results derived from the cross sections. The overall agreement between the present semiempirical results and those of Ref. [22] is, however, rather good and they are both close to the predictions of the ECB model.

The results in Fig. 5 are obtained by assuming capture to unscreened hydrogenlike states and taking the binding energy of the rth transferred electron to be

$$E_r = \frac{q^2}{2(n_r^*)^2}. \tag{8}$$

TABLE III. Same as Table I, but with Xe as a target.

q	$\sigma^1_{q,q-1}$	$\sigma^2_{q,q-1}$	$\sigma^3_{q,q-1}$	$\sigma^4_{q,q-1}$	$\sigma^5_{q,q-1}$	$\sigma^6_{q,q-1}$
14	9.9±0.4					
15	12.1±0.6	7.2±0.4	3.3±0.2	1.4±0.9		
19	11.9±1.8					
20	14.9±0.7	8.3±0.4	4.6±0.2	2.7±0.2	1.2±0.09	0.2±0.05
24	17.4±1.3					
25	17.5±1.0	8.2±0.5	4.5±0.3	2.6±0.2	1.6±0.2	0.5±0.08
27	25.8±3.2					
28	17.6±0.9	9.4±0.5	5.0±0.3	2.7±0.2	1.6±0.1	0.9±0.08
29	23.1±2.1					
30	20.9±1.2	10.7±0.7	4.7±0.4	2.8±0.2	1.4±0.1	0.6±0.08
31	19.3±2.1	9.1±1.1	4.5±0.6	2.2±0.3		
32	24.4±1.4	11.1±0.9	4.7±0.4	3.2±0.3	1.2±0.2	
34	21.9±3.5					
35	21.3±3.2	8.4±1.4	3.5±0.6	1.6±0.4	1.2±0.3	0.7±0.2
36	25.3±4.5	10.0±1.8	4.8±0.9	2.0±0.4	1.2±0.3	
37	28.8±4.2	12.2±2.0	4.8±0.9	1.6±0.4		
q	$\sigma^2_{q,q-2}$	$\sigma^3_{q,q-2}$	$\sigma^4_{q,q-2}$	$\sigma^5_{q,q-2}$	$\sigma^6_{q,q-2}$	$\sigma^7_{q,q-2}$
15	0.2±0.03	0.4±0.04	0.8±0.06	1.3±0.08	1.0±0.07	
20	0.8±0.1	1.8±0.2	1.8±0.2	1.8±0.2	1.5±0.2	
25	1.3±0.2	1.7±0.2	2.0±0.2	2.0±0.2	1.4±0.2	1.0±0.1
28	0.8±0.08	1.3±0.1	1.5±0.1	1.2±0.09	1.2±0.09	0.7±0.07
30	2.0±0.2	2.8±0.2	2.7±0.2	2.0±0.2	1.6±0.2	0.9±0.09
31	3.1±0.4	3.6±0.4	2.5±0.3	2.4±0.3	2.0±0.3	1.6±0.2
32	4.6±0.4	5.0±0.5	4.8±0.4	3.6±0.4	3.0±0.3	2.0±0.2
35	5.3±0.9	6.3±1.1	4.4±0.8	3.5±0.6	1.6±0.4	
36	5.1±1.0	4.5±0.8	3.9±0.7	2.4±0.5		
37	6.2±1.1	6.2±1.1	5.1±0.9	2.8±0.6	1.9±0.4	
q	$\sigma^8_{q,q-2}$	$\sigma^9_{g,g-2}$	$\sigma^3_{q,q-3}$	$\sigma^4_{q,q-3}$	$\sigma^5_{q,q-3}$	$\sigma^6_{q,q-3}$
20			0.5±0.09	0.8±0.1	1.1±0.1	
28	0.5±0.06	0.5±0.05	0.1±0.03	0.2±0.03	0.3±0.04	0.5±0.05
30	0.7±0.08	0.4±0.06	0.3±0.06	0.4±0.07	0.5±0.07	1.0±0.1
31	0.6±0.02					
32	1.4±0.2	0.6±0.1	0.4±0.09	0.4±0.09	0.8±0.1	0.7±0.1

This is well justified when q is high. Note that Eq. (7) is derived under the assumption that earlier transferred electrons (to the projectile) screen the projectile charge completely as ''seen'' by the next electron to be transferred from the target. This is fully consistent with using Eq. (8), which assumes no screening by earlier transferred electrons when the active electron becomes localized to the projectile (i.e., when the transfer of the rth electron is completed). Here we obtain the model prediction of the effective quantum states populated in one- and two-electron removal from

$$n_1^* = \frac{q}{\sqrt{2\left(\frac{q-1}{R_1} + I_1\right)}} \tag{9}$$

and

$$n_2^* = \frac{q}{\sqrt{2\left(\frac{q-3}{R_2} + I_2\right)}}. \tag{10}$$

Using Eq. (6), we arrive at the two expressions for the experimental crossing radii R_1^{ex} and R_2^{ex},

$$^{ex}\sigma_q^{\mathrm{tot}} = \pi (R_1^{ex})^2 \tag{11}$$

and (starting the sum at $r=2$)

$$^{ex}\sigma_q^{r\geq 2} = \pi (R_2^{ex})^2. \tag{12}$$

Inserting R_1^{ex} and R_2^{ex} into Eqs. (9) and (10), respectively, gives the semiempirical values for n_1^* and n_2^* (cf. Fig. 5). The cross section for removing *at least* two electrons from the target is denoted $^{ex}\sigma_q^{r\geq 2}$ and for Ar and Xe these quantities differ from $^{ex}\sigma_q^2$. One should bear in mind that the

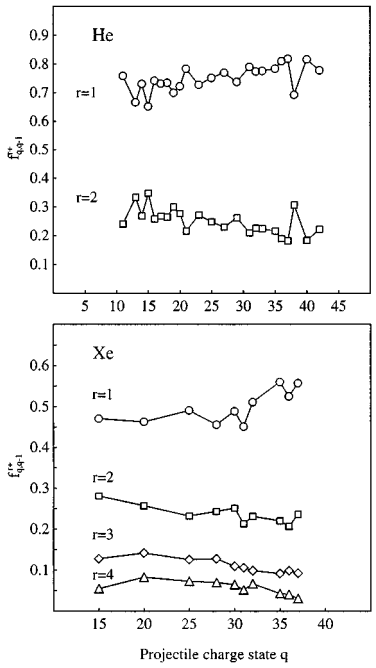

FIG. 3. Partial charge-state fractions $f^r_{q,q-1}$ for $r+$ recoil ions in coincidence with projectiles in final charge state $(q-1)+$ as functions of the incoming projectile charge q. Data are displayed for targets of He (top) and Xe (bottom) and show that the fractions are varying slowly with q. That is, $f^r_{q,q-1} \sim f^r_{q-1,q-2}$ for neighboring charge states.

semiempirical n_1^* and n_2^* results of Fig. 5 are deduced using the ECB model. An agreement with direct evaluations of this model is thus not very strong support for the model. However, the comparison shows that it is possible to use the measured absolute cross sections in order to deduce rather good estimates of the capture states. This is warranted by the fair agreement with the Q-value-based results of Ref. [22]. Finally, the present semiempirical n_2^* values should be taken as upper limits since the procedure we have used here does not take a possible rearrangement of the outer electron into

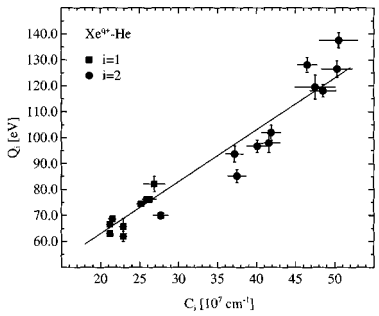

FIG. 4. Experimental Q_1 and $Q_2 = Q_2^{\rm tot} - Q_1^{\rm tot}$ values for Xe^{q+}-He collisions from Ref. [21] plotted as functions of C_1 and C_2, respectively (cf. the text).

account. Such a rearrangement is likely to occur since the screening of the core for the first transferred electron will change when the second electron is captured inside it ($n_2^* \leqslant n_1^*$) [21].

B. Ratios of electron-removal cross sections

In the previous subsection we found reasonable agreement between the present experimental results for $\sigma_q^{\rm tot}$, n_1^*, and n_2^* and the corresponding ECB predictions for all three target gases He, Ar, and Xe. However, measurements of cross section ratios σ_q^2/σ_q^1 provide much more sensitive tests of the model, which can easily be seen from Eqs. (9) and (10) indicating that $\sigma_q^2/\sigma_q^1 \sim (n_2/n_1)^4$.

It has been observed before that the ECB model gives good results for the ratio between the cross sections for two- and one-electron removal from Xe, while the corresponding values for the He target in general are a factor of 2 off [14,28]. Early on there was an attempt to explain this difference as due to a special transfer excitation (TE) mechanism, in which one electron was transferred to the projectile while the other target electron was excited [27]. This process was assumed to be active for He, but not for the heavier targets. The reason for this was that recapture (from the projectile to

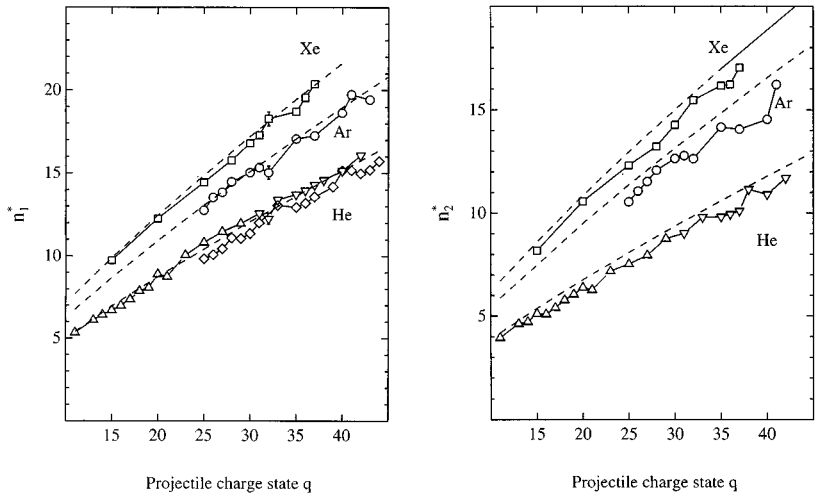

FIG. 5. Effective principal quantum states populated by the first ${}^{ex}n_1^*$ and the second ${}^{ex}n_2^*$ transferred electron as functions of q for targets of He, Ar, and Xe. The dashed lines represent the ECB model.

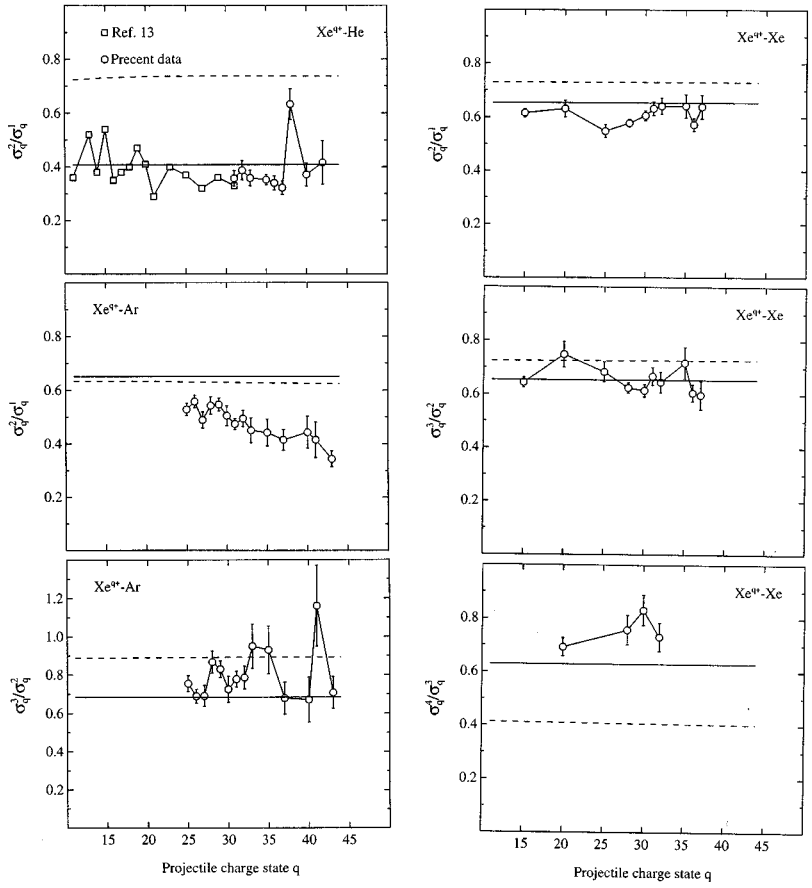

FIG. 6. Ratios between the electron-removal cross section $\sigma_q^{r+1}/\sigma_q^r$ in Xe^{q+}-He, Xe^{q+}-Ar, and Xe^{q+}-Xe collisions as a function of the incoming projectile charge q. The dashed lines are the ECB predictions and the full lines are due to the recently developed scaling law [see Eq. (13) and Ref. [19]].

the target) only was considered to be efficient if two but not three electrons could leave the target. An attempt to isolate this target-specific transfer excitation process experimentally for He was then made using the translational energy-gain method. The TE process was expected to have the same charge-state signatures as single-electron capture, but with a smaller-Q value. In that work [22] no clear evidence of TE at the cross-section level predicted by theoretical considerations [27] was found, but it could not be completely ruled out that the process could be active at a somewhat more modest level ($\sim 5-10\,\%$ of single-electron capture). This would, however, be insufficient in order to explain the low experimental σ_q^2/σ_q^1 ratio for He. Instead, it was suggested that the finite density of capture states for transfer of a second electron from He could make the measured ratio deviate from the model predictions using quasicontinua of projectile capture states. This conclusion was tentatively derived from the measured mean-Q values for single-electron capture in Xe^{q+}-He collisions [22].

Using various reductions of the data presented in Tables I–III, we recently derived [19] a semiempirical formula for the absolute cross sections for removing exactly r electrons from the target:

$$^{se}\sigma_q^r = (2.7\times 10^{-13})qr \Big/ I_1^2 I_r^2 \sum_{j=1}^{N} (j/I_j^2), \qquad (13)$$

where the result is in cm^2 if the ionization potentials I_j are given in eV. This formula was obtained by means of fits to the experimental data in [19], but Eq. (13) could also be expressed approximately using the R_r values (4) of the ECB model

$$^{se}\sigma_q^r \approx \frac{\pi R_r^2}{\Sigma_{j=1}^{N} j(I_1/I_j)^2}. \qquad (14)$$

The sums over j in Eqs. (13) and (14) run over the number of outer-shell electrons N. In this context we wish to stress that the results obtained from Eq. (14) may be very different from the ones obtained from the ECB model (5). For example, relative recoil-ion charge-state distributions deduced from Eqs. (13) or (14) are found to be in excellent agreement with the present experimental results for He, Ar, and Xe [19]. The same quantities derived from Eq. (5) give reasonable results for Ar and Xe but fail for He. Thus, in contrast to the ECB model, Eq. (13) is able to reproduce the experimental results for σ_q^2/σ_q^1 both for light and heavy targets. The scaling law (13) is only partly consistent with the basic views of the charge-transfer process used in the ECB model. The main difference is that whereas the ECB model assumes that r-electron transfer takes place with a probability of one for impact parameters between R_r and R_{r+1}, Eq. (13) is consis-

tent with a picture where r or fewer than r electrons are removed from the target for the same impact parameter range [19].

In Fig. 6 we show the cross section ratios σ_q^2/σ_q^1 (for He, Ar, and Xe), σ_q^3/σ_q^2 (only Ar and Xe), and σ_q^4/σ_q^3 (only Xe). The experimental ratios σ_q^3/σ_q^2 and σ_q^4/σ_q^3 in Fig. 6 are not, except in a few cases, the complete ratios since $\sigma_{q,q-3}^3$, i.e., true three-electron capture, and $\sigma_{q,q-4}^4$, i.e., true four-electron capture, are missing in σ_q^3 and σ_q^4, respectively. We have measured the ''true'' ratio σ_q^3/σ_q^2 for Xe^{q+}-Xe in four cases $q=20$, 28, 30, and 32. From this we conclude that the contribution from true three-electron capture $\sigma_{q,q-3}^3$ to three-electron removal σ_q^3 is small ($\sim 3-4\%$). Also, it seems reasonable to assume that we can extend this argument further and that the $\sigma_{q,q-4}^4$ part in σ_q^4 can be neglected. For He and Xe all ratios are clearly much better described by the recently developed scaling rule (full lines in Fig. 6) than by the ECB model (dashed lines). For Ar, however, the two predictions from [19] and [8] appear to be equally successful. An inspection of the individual σ_q^r cross sections show, however, that formulas (13) and (14) give somewhat better results than the ECB model, as can be seen in Ref. [19].

C. Electron-retainment cross sections

The electron-retainment cross sections are defined by $\sigma_{q,q-p}=\Sigma_r \sigma_{q,q-p}^r$, where the sum runs over all produced recoil-ion charge states $r+$ for a given value of p. Here we will in particular discuss the cases $p=1$ and $p=2$. When Müller and co-workers [6,7] derived their famous scaling law more than fifteen years ago only data for rather moderate projectile charge states (mostly below $q=10$) were available. Nakamura *et al.* [18] have recently measured $\sigma_{q,q-p}$ for I^{q+}-B, $q=10,15$ and $p=1-3$, colliding with various multi-electron targets B and compared these with the scaling cross sections $\sigma_{q,q-p}^{MS}=A_p q^{\alpha_p} I_1^{\beta_p}$ (with, e.g., $\alpha_1=1.17$ and $\beta_1=-2.76$). They [18] found fair agreement for $p=1$, but for $p=2$ there was a significant deviation, which became even more pronounced for $p=3$. In Fig. 7 we have compared the present high-q data with the predictions of $\sigma_{q,q-p}^{MS}$ [6,7] as functions of q. The agreement between the measured cross sections and $\sigma_{q,q-1}^{MS}$ is rather good for He, while the same comparisons for the heavier targets are much less successful. The $\sigma_{q,q-1}^{MS}$ values for Ar and Xe lie above the experimental cross sections and the deviations increase with q as is seen in Fig. 7. Note that this conclusion is different from the one reached by Nakamura *et al.* [18], who used only projectiles of charge states $q=10$ and $q=15$ and found fair agreement for all targets and $p=1$. The present observations are explained as follows. (i) Multiple-electron removal from He amounts to only $\sim 30\%$ of the total-reaction cross section. A large part of the two-electron-removal cross section will further contribute to $\sigma_{q,q-1}$ due to the dominance of transfer ionization at the present velocities. True double-electron capture will at most amount to about 15% of $\sigma_q^{\rm tot}$ in the present charge-state regime due to the fact that the probability for radiative stabilization is lower than 50% [26,29]. Thus $\sigma_{q,q-1}$ for He will develop essentially as the total experimental reaction cross section and since $\sigma_q^{\rm tot}$ scales linearly

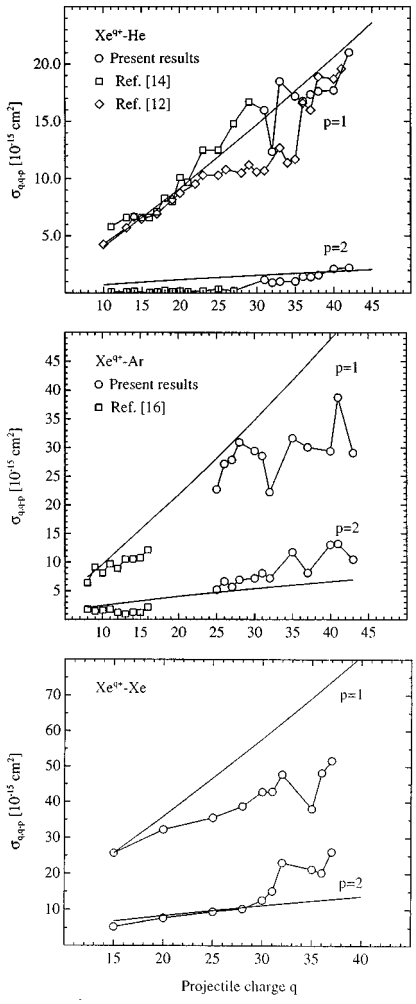

FIG. 7. Cross sections $\sigma_{q,q-p}$ for retaining p ($p=1$ and 2) electrons as functions of q for all three targets. The results from Andersson *et al.* [14] are also included. In the He target case also I^{q+}-He data from Iwai *et al.* [11] is included. The full lines are due to the scaling cross sections $\sigma_{q,q-p}^{MS}$ (cf. the text and Refs. [6,7]).

with q as shown in [19] it is also rather well described by $\sigma_{q,q-1}^{MS}$, which scale as $q^{1.17}$. (ii) Multiple-electron removal amounts to 60–70 % of $\sigma_q^{\rm tot}$ for Ar and Xe. In addition, stabilization of two (or more) electrons on the projectile becomes more likely as the number of initially transferred electrons increases, as it can only do for targets heavier than He. Both these effects tend to increase $\sigma_{q,q-2}$ at the expense of $\sigma_{q,q-1}$. This feature becomes more pronounced when q increases as the probability of radiative stabilization becomes larger in this q region and it accounts for the observed saturations of the experimental $\sigma_{q,q-1}$ cross sections for Ar and Xe. The same reasons also explain the deviations between experimental cross sections and the (close to) $q^{0.71}$ scaling of $\sigma_{q,q-p}^{MS}$ for $p=2$, which are evident from Fig. 7. So far, no scaling law for electron-retainment cross sections that is generally valid both for heavy and light targets and for high and low projectile charge has been established. However, in Ref. [19] we presented two separate scaling relations: one that appears to be valid for light targets (i.e., He) and one that appears to be valid for heavy targets (i.e., Ar and Xe).

V. CONCLUSION

The main results presented here are the close to 300 absolute reaction cross sections for single- and multiple-electron transfer processes in slow collisions between highly charged Xe ions and targets of He, Ar, and Xe. The experimental technique has been described in some detail and special emphasis has been given to the procedure used in order to determine the different effective target lengths for the different gases. We have also described the extraction of single-electron-capture cross sections for the collision system $Xe^{(q-1)+}$-B from double-collision rates measured for Xe^{q+}-B collisions. This was necessary in order to resolve a problem in the data analysis, which was due to ''tail and hump intensities'' close to the primary peak.

The present collection of data is easily the largest one presented for slow collisions involving ions of high charge. In addition, unlike all previous sets of such data, it contains charge-state coincidences for both light and heavy targets. The measured absolute r-electron-removal cross sections were used in order to deduce semiempirical effective quantum numbers for transfer of the first and the second electron from the target to the projectile. These semiempirical results and the experimental ones for the total reaction cross sections compare favorably with the extended classical over-the-barrier model. However, comparisons between predictions from the same model and ratios of experimental cross sections for $(r+1)$- and r-electron removal exposed some rather serious discrepancies especially for the He target. We also made similar comparisons using a different semiempirical expression for r-electron removal from the target and found significantly better agreement with the experimental data for He and Xe. In fact, the recently developed scaling law is able to account for all observed features of the present data (see also Ref. [19]), except the σ_q^2/σ_q^1 and σ_q^3/σ_q^2 data for Ar. This is, however, a rare exception, and although this particular problem still is unexplained, the general success of the scaling law indicates that the one-to-one correspondence between the number of removed target electrons and the impact parameter used in the ECB model has to be reconsidered. This and the motivation for the scaling law are discussed in more detail in the related article by Selberg *et al.* [19].

ACKNOWLEDGMENT

This project was supported by the Swedish National Science Research Council (NFR).

[1] J. J. Thomson, *Rays of Positive Electricity and Their Applications to Chemical Analysis* (Longmans, Green, London, 1913), p. 46.
[2] A. Niehaus, Comments At. Mol. Phys. **9**, 153 (1980).
[3] C. L. Cocke, R. Dubois, T. J. Gray, E. Justinianov, and C. Can, Phys. Rev. Lett. **46**, 1671 (1981).
[4] W. Groh, A. Müller, C. Achenbach, A. S. Schlachter, and E. Salzborn, Phys. Lett. **85A**, 77 (1981).
[5] M. N. Panov, A. A. Basalaev, and K. O. Lozhkin, Phys. Scr. **T3**, 124 (1983), and references therein.
[6] A. Müller and E. Salzborn, Phys. Lett. **62A**, 391 (1977).
[7] A. Müller, C. Achenbach, and E. Salzborn, Phys. Lett. **70A**, 410 (1979).
[8] A. Bárány, G. Astner, H. Cederquist, H. Danared, S. Hult, P. Hvelplund, A. Johnson, H. Knudsen, L. Liljeby, and K.-G. Rensfelt, Nucl. Instrum. Methods Phys. Res. B **9**, 397 (1985).
[9] H. Ryufuku, K. Sasaki, and T. Watanabe, Phys. Rev. A **21**, 745 (1980).
[10] A. Niehaus, J. Phys. B **19**, 2925 (1986).
[11] T. Iwai, Y. Kaneko, M. Kimura, N. Kobayashi, A. Matsumoto, S. Ohtani, K. Okuno, S. Takagi, H. Tawara, and S. Tsurubuchi, J. Phys. B **17**, L95 (1984).
[12] H. Tawara, T. Iwai, Y. Kaneko, M. Kimura, N. Kobayashi, A. Matsumoto, S. Ohtani, K. Okuno, S. Takagi, H. Tawara, and S. Tsurubuchi, J. Phys. B **18**, 337 (1985).
[13] R. Mann, Z. Phys. D **3**, 85 (1986).
[14] H. Andersson, G. Astner, and H. Cederquist, J. Phys. B **21**, L187 (1988).
[15] J. Vancura, V. J. Marchetti, J. J. Perotti, and V. O. Kostroun, Phys. Rev. A **47**, 3758 (1993).
[16] J. Vancura, J. J. Perotti, J. Flidr, and V. O. Kostroun, Phys. Rev. A **49**, 2515 (1994).
[17] R. Ali, C. L. Cocke, M. L. A. Raphaelian, and M. P. Stöckli, Phys. Rev. A **49**, 3586 (1994).
[18] N. Nakamura, F. J. Currell, A. Danjo, M. Kimura, A. Matsumoto, S. Ohtani, H. A. Sakaue, M. Sakurai, H. Tawara, H. Watanabe, I. Yamada, and M. Yoshino, J. Phys. B **28**, 2959 (1995).
[19] N. Selberg, C. Biedermann, and H. Cederquist, Phys. Rev. A **54**, 4127 (1996).
[20] M. Kimura, N. Nakamura, H. Watanabe, I. Yamada, A. Danjo, K. Hosaka, A. Matsumoto, S. Ohtani, H. A. Sakaue, M. Sakurai, H. Tawara, and M. Yoshino, J. Phys. B **28**, L643 (1995).
[21] H. Cederquist, C. Biedermann, N. Selberg, and P. Hvelplund, Phys. Rev. A **51**, 2169 (1995).
[22] H. Cederquist, C. Biedermann, N. Selberg, and P. Hvelplund, Phys. Rev. A **51**, 2191 (1995).
[23] N. Selberg, C. Biedermann, and H. Cederquist (unpublished).
[24] M. L. A. Raphaelian, M. P. Stöckli, W. Wu, and C. L. Cocke, Phys. Rev. A **51**, 1304 (1995).
[25] H. Cederquist, C. Biedermann, N. Selberg, E. Beebe, M. Pajek, and A. Bárány, Phys. Rev. A **47**, R4551 (1993).
[26] H. Cederquist, H. Andersson, E. Beebe, C. Biedermann, L. Broström, Å. Engström, H. Gao, R. Hutton, J. C. Levin, L. Liljeby, M. Pajek, T. Quinteros, N. Selberg, and P. Sigray, Phys. Rev. A **46**, 2592 (1992).
[27] H. Cederquist, Phys. Rev. A **43**, 2306 (1991).
[28] H. Cederquist, E. Beebe, C. Biedermann, Å. Engström, H. Gao, R. Hutton, J. C. Levin, L. Liljeby, T. Quinteros, N. Selberg, and P. Sigray, J. Phys. B **25**, L69 (1992).
[29] H. Cederquist, C. Biedermann, N. Selberg, L. Liljeby, and E. Beebe, Phys. Scr. **T46**, 218 (1993).